An Extended Frequency-Domain Passivity Theory for MIMO Dynamics Specifications of Voltage-Source Inverters

Feifan Chen, *Student Member, IEEE*, Sei Zhen Khong, *Senior Member, IEEE*, Lennart Harnefors, *Fellow, IEEE*, Xiongfei Wang, *Fellow, IEEE*, Dan Wang, *Member, IEEE*, Henrik Sandberg, *Fellow, IEEE*, Liang Zhao, *Member, IEEE*, Mikko Routimo, *Member, IEEE*, Jarno Kukkola, Kin Cheong Sou, *Member, IEEE*, and Karl Henrik Johansson, *Fellow, IEEE*

***Abstract*—In grid-connected inverter systems, frequency-domain passivity theory is increasingly employed to analyze grid–inverter interactions and guide inverter control designs. However, due to difficulties in meeting sufficient passivity-based stability conditions at low frequencies, passivity theory often falls short of achieving stable system specifications. This article introduces an extended frequency-domain passivity theory. By incorporating a weighting matrix, an extended stability condition is derived. Compared to conventional passivity-based stability conditions, the proposed theory significantly reduces conservativeness and is more suited for analyzing grid–inverter interactions and guiding inverter control design. Theoretical analyses, numerical examples, and experimental results are provided to validate the effectiveness of the proposed methods.**

***Index Terms*—Control design, grid-connected inverters, passivity, stability.**

I. Introduction

GRID-CONNECTED inverters are commonly found in modern power systems [1], where wide-band oscillation issues arising from the interaction between inverters and the grid have attracted increasing attention [2]. Passivity theory is a widely used and intuitive tool for inverter control design, and stability assessment of the system [3], [4], especially when there exists uncertainties in the grid impedance. From the energy perspective, a passive component only dissipates or stores energy without generating it. Examples of passive components include resistors, inductors, and capacitors. When all subsystems within a system are passive, the system is stable, regardless of the complexity of the interactions among the subsystems [5]. Therefore, achieving passive grid-connected inverters through reasonable design is a highly desirable goal that prevents wide-band oscillations caused by adverse inverter–grid interactions. In the frequency domain, based on the different impedance representations, the passivity degree of an inverter at a specific frequency can be quantified by the real part value or the passivity index of its input admittance [5], [6].

The impedance modeling of grid-connected inverters can be divided into high-frequency and low-frequency categories based on the frequency coupling characteristics of controllers across different frequency bands [3]. Passivity-based analysis also exhibits distinct features in these different frequency ranges. For the analysis of high-frequency ($\omega \geq 2.0$ p.u.) oscillations, the main destabilizing factors are the time delay introduced by the computation and pulsewidth modulation (PWM), and the current control (CC) dynamics [3]. The slow dynamics from the synchronization control (SC) and power control (PC), are often ignored, and thus the inverter can be modeled as a single-input single-output (SISO) system [7]. The impacts of the CC and time delay can be characterized as a negative resistance region in the impedance, which introduces negative damping to the system [3]. By introducing a voltage feedforward control [8] or reducing the time delay [9], [10], the negative resistance region of the inverter in the high-frequency range can be eliminated, thereby avoiding potential instability.

At low frequencies (around $\omega = 0$ in the dq frame), the outer loops, such as a phase-locked loop (PLL) or PC, are not simply d-to-d and q-to-q symmetric. These controls introduce complex coupling between the d-axis and q-axis, making the equivalent admittance of the inverter a multiple-input multiple-output (MIMO) system [6], [11]. In this case, the passivity degree of the inverter can be quantitatively assessed by the passivity index [5], [12]. Assuming that the grid impedance is passive, the stability

Received 12 June 2024; revised 19 September 2024; accepted 27 October 2024. Date of publication 30 October 2024; date of current version 18 December 2024. The work of Sei Zhen Khong was supported by the National Science and Technology Council of Taiwan under Grant 113-2222-E-110-002-MY3. Recommended for publication by Associate Editor Q. Shafiee. *(Corresponding author: Xiongfei Wang.)*

Feifan Chen, Xiongfei Wang, Dan Wang, Henrik Sandberg, Liang Zhao, and Karl Henrik Johansson are with the School of Electrical Engineering and Computer Science, KTH Royal Institute of Technology, 10044 Stockholm, Sweden (e-mail: feifanc@kth.se; xiongfei@kth.se; danwang@kth.se; hsan@kth.se; liazhao@kth.se; kallej@kth.se).

Sei Zhen Khong and Kin Cheong Sou are with the Department of Electrical Engineering, National Sun Yat-sen University, Kaohsiung City 80424, Taiwan (e-mail: szkhong@mail.nsysu.edu.tw; sou12@mail.nsysu.edu.tw).

Lennart Harnefors is with the ABB Corporate Research, 72226 Västerås, Sweden (e-mail: lennart.harnefors@se.abb.com).

Mikko Routimo and Jarno Kukkola are with the ABB Oy Drives, 00380 Helsinki, Finland (e-mail: mikko.routimo@fi.abb.com; jarno.kukkola1@fi.abb.com).

Color versions of one or more figures in this article are available at https://doi.org/10.1109/TPEL.2024.3488853.

Digital Object Identifier 10.1109/TPEL.2024.3488853

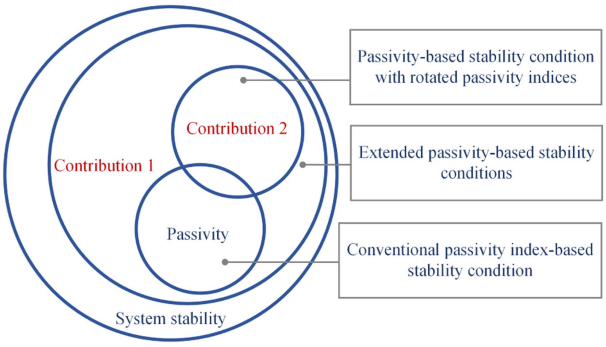

Fig. 1. Relationships among system stability, conventional passivity-based stability conditions, and the two contributions.

conditions[1] for grid-connected inverter systems based on the passivity index in the low-frequency range are: 1) the passivity index of the inverter is non-negative [13], or 2) the passivity index of the inverter is negative but excess passivity from the grid impedance can compensate for the deficiency of the inverter passivity [5].

However, meeting either of these two conditions is challenging [14], mainly due to two limitations. First, the passivity index of the inverter is inherently negative in the low-frequency region, which is difficult to eliminate [15]. In [16] and [17], it is found that the presence of the integrator in the voltage control can even result in a negative infinity value. Second, the excess passivity from the grid impedance is often considered zero from a robustness perspective [12]. Therefore, a common practice in the low-frequency range is to associate the passivity degree of the inverter with the system stability robustness [3], [14], [18], i.e., the system is expected to have better stability robustness by improving the passivity degree. Two metrics can be used to evaluate the passivity degree from the passivity index plot: first, the width of the frequency region where the passivity index is negative [3], and second, the minimum value of the passivity index [12]. Recent research has found pitfalls in the two passivity degree metrics [16]. It remains unclear which one of the two metrics is more suitable for characterizing the passivity degree at low frequencies, and these two metrics may even be in conflict with each other. It has been discovered that focusing on only one indicator, either simply reducing the frequency region of the negative passivity index or increasing the minimum value of the passivity index, may reduce the system stability robustness and even result in system instability [17].

This article aims to address the limitations of using the frequency-domain passivity theory to guide inverter control design and verify system stability in the low-frequency range. The relationships among system stability, conventional passivity-based stability conditions, and the two contributions of this article are shown in the Venn diagram in Fig. 1. First, the conventional stability conditions based on passivity theory are extended. The proposed extension provides a larger framework than conventional passivity theory by adding flexibility through the inclusion of a weighting matrix when defining the passivity index. This allows for a more flexible decomposition of the dynamics of inverters and the grid. The second contribution lies in the specific choice of a rotation matrix as the weighting matrix within the extended passivity theory framework. This results in a new passivity index, termed the *rotated passivity index*, which is particularly effective for specifying low-frequency dynamics and guiding inverter control design. Compared to the conventional passivity index, the stability conditions based on the rotated passivity index exhibit significantly reduced conservativeness when applied to grid-connected inverter systems. This means that the new index, along with the associated stability conditions, provides a practical criterion for ensuring the closed-loop system stability and system-stabilizing inverter control specifications. Moreover, the proposed index is as straightforward as the conventional one and remains within the framework of generalized passivity theory. It introduces no additional theoretical complexities, thereby avoiding the potential difficulties and high complexity that can arise when employing multiple theoretical tools for system dynamics specification in practical applications.

The rest of this article is organized as follows. In Section II, the preliminaries of grid-connected inverters and the passivity theory are presented. In Section III, the basic principles of the proposed extended passivity frequency domain passivity theory are introduced, along with the stability conditions and a general guideline. In Section IV, the rotated passivity index is proposed, which is utilized in the subsequent sections. In Sections V and VI, the effectiveness and superiority of the rotated passivity index over the conventional passivity index in terms of dynamic specification and control design guidance are shown through examples of both PLL-synchronized and PC-synchronized inverters. In Section VII, a comprehensive discussion is presented, primarily covering the system uncertainties, comparisons with other multivariable theories, and the limitations of the proposed theory. Experimental validations are provided in Section VIII. Finally, Section IX concludes this article.

II. Preliminaries

A. Grid-Connected Inverter System

Fig. 2 shows the schematic diagram of a grid-connected inverter system. On the inverter side, it consists of a set of controllers and an output filter. The controllers include CC, alternating voltage control (AVC), reactive power control (RPC), and SC. In this article, SC refers to the PLL in Sections V and PC in Section VI, respectively. The output filter is typically an inductive–capacitive filter, but the influence of capacitance at low frequencies is negligible [19]. The detailed configurations of the controllers for PLL-synchronized and PC-synchronized inverters are presented in Figs. 3 and 4, respectively. The PLL is proportional and has a gain of α_p/E_0, where α_p represents the PLL bandwidth. First-order low-pass filters $H(s)$, $H_1(s)$, and $H_2(s)$ feature a bandwidth of α_f. R_a is the CC gain, configured as $\alpha_c L$, where α_c denotes the desired CC loop bandwidth and L is the output filter inductance [13]. The PC is also proportional, and the design of its gain is aligned with [20]. On the grid side, grid

[1]The marginally stable case is included.

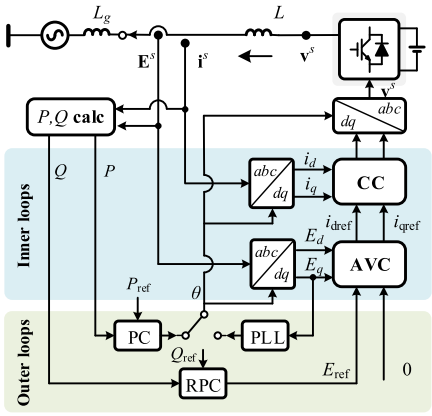

Fig. 2. System configuration and block diagram of a grid-connected inverter.

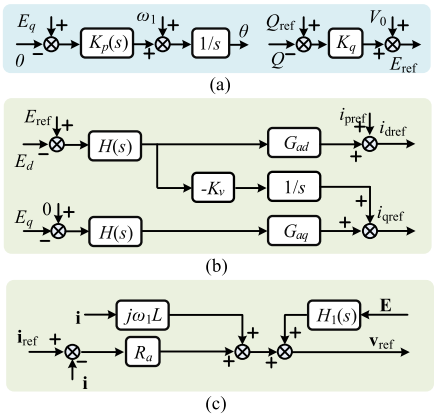

Fig. 3. Controller structure of PLL-synchronized inverter. (a) PLL and Q-V droop. (b) AVC. (c) CC.

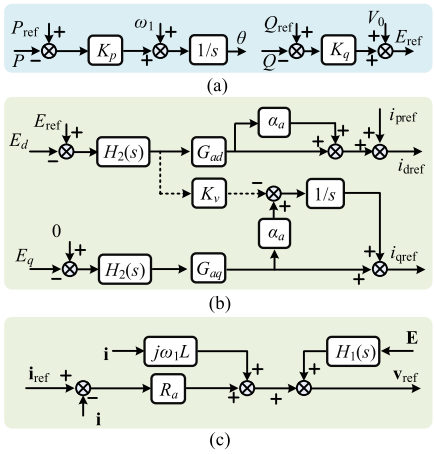

Fig. 4. Controller structure of PC-synchronized inverter. (a) P-f droop and Q-V droop. (b) AVC. (c) CC.

impedance is characterized by inductance L_g, with negligible resistance R_g [12].

Passivity-based analysis in frequency domain requires system impedance modeling [13]. In this article, the inverter is modeled as an ideal current source in parallel with an admittance $\mathbf{Y}$, while the grid is modeled as an ideal voltage source in series with an impedance $\mathbf{Z}_g$. The corresponding circuit representation is given

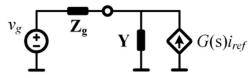

Fig. 5. System circuit representation of the grid-connected systems.

in Fig. 5. In the testbench used in this study, the dc-side voltage is provided by a dc voltage source. In practical applications, the dc-side voltage can be supplied by a back-to-back converter or an energy storage unit, such as a GFM-BESS [21]. This setup decouples the dc-side dynamics from the inverter of interest. As a result, the dynamics from the dc side are not considered. In addition, since this study primarily focuses on low-frequency behavior, the high-frequency dynamics caused by delays are also not considered [12]. The impedance modeling method for grid-connected inverters has been widely discussed, and this article adopts the modeling process from [6], [12], [22], and [23] without a further discussion.

B. Passivity Theory

A MIMO system (real-rational transfer function) is said to be exponentially stable if all its poles are located in the open left-half complex plane. It is said to be marginally stable if all its poles are located in the closed left-half complex plane and any poles on the imaginary axis are simple. A system is called stable if it is either exponentially stable or marginally stable, and unstable if it is not stable in this work. It is said to be minimum phase if all its zeros are located in the open left-half complex plane.

Given a general matrix $\mathbf{M} \in \mathbb{C}^{n\times n}$, its complex conjugate transpose is denoted by $\mathbf{M}^H$. $\mathbf{M}$ is said to be Hermitian if $\mathbf{M} = \mathbf{M}^H$. When this is the case, $\mathbf{M} > xI$ for some $x \in \mathbb{R}$ implies $\min \lambda[\mathbf{M}] > x$, where λ denotes the eigenvalue of $\mathbf{M}$. $\mathbf{M}$ is said to be positive definite if $\mathbf{M} > 0$.

For an exponentially stable and minimum phase MIMO system $\mathbf{G}(s)$, according to [5], the input feedforward passivity (IFP) index at frequency ω, denoted as $\nu_F[\mathbf{G}(s), \omega]$, is defined as

$$\frac{1}{2}\min \lambda \left[\mathbf{G}\left(j\omega\right) + \mathbf{G}^H\left(j\omega\right)\right] \tag{1}$$

and the output feedback passivity (OFP) index at frequency ω, denoted as $\rho_F[\mathbf{G}(s), \omega]$, is defined as

$$\frac{1}{2}\min \lambda \left[\mathbf{G}^{-1}\left(j\omega\right) + \mathbf{G}^{-H}\left(j\omega\right)\right] \tag{2}$$

where $\min \lambda$ is the minimum eigenvalue and the superscript H is the Hermitian operator, i.e., transpose–conjugate. $\mathbf{G}(s)$ is said to be passive if ν_F (or ρ_F) $\geq 0, \forall \omega \geq 0$. For a general MIMO interconnected negative-feedback system $[\mathbf{G}_1, \mathbf{G}_2]$ shown in Fig. 6(a), if $\mathbf{G}_1$ and $\mathbf{G}_2$ are passive, $[\mathbf{G}_1, \mathbf{G}_2]$ is stable. The passivity-based stability conditions can be extended to nonpassive systems [5], [24]. The underlying idea is that within an interconnected system, there exist both passive and nonpassive subsystems. If the surplus passivity in the passive subsystem can offset the passivity deficit in the nonpassive system, then the closed-loop system is stable [5]. More specifically, the feedback system is exponentially stable, if $\mathbf{G}_1$ is exponentially stable and

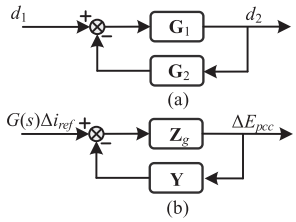

Fig. 6. Interconnected feedback system of (a) [$\mathbf{G}_1$, $\mathbf{G}_2$]. (b) [$\mathbf{Z}_g$, $\mathbf{Y}$].

$\mathbf{G}_2$ is exponentially stable and minimum-phase, and

$$\nu_F\left[\mathbf{G}_1(s),\omega\right]+\rho_F\left[\mathbf{G}_2(s),\omega\right]>0,\forall\omega\geq 0. \tag{3}$$

This extension reduces the conservatism of the original passivity-based stability condition, enabling the continued applicability of the passivity-based theory even in cases where certain subsystems are not passive.

The grid-connected inverter system in Fig. 5 can also be modeled as an interconnected negative feedback system, as shown in Fig. 6(b), which is denoted as [$\mathbf{Y}$, $\mathbf{Z}_g$], where $\mathbf{Y}$ is typically stable but may be a nonminimum-phase system [12], [25], and $\mathbf{Z}_g$ (passive components) is exponentially stable and a minimum-phase system. Therefore, according to (3), [$\mathbf{Y}$, $\mathbf{Z}_g$] is exponentially stable if $\mathbf{Y}$ is exponentially stable and

$$\nu_F\left[\mathbf{Y}(s),\omega\right]+\rho_F\left[\mathbf{Z}_g(s),\omega\right]>0,\forall\omega\geq 0. \tag{4}$$

However, typically from a robustness perspective, contributors to the excess passivity in $\mathbf{Z}_g$, such as line resistance, are considered to be zero [12]. Therefore, when using passivity theory to guide inverter control design to ensure system stability, it is necessary to have the equivalent admittance of the inverter, $\forall\omega\geq 0$, satisfy

$$\nu_F\left(\mathbf{Y}(s),\omega\right)>0. \tag{5}$$

However, as discovered in numerous studies [3], [14], [26], its hard to obtain condition (5) that are feasible in practice. In such cases, stability assessments or control designs based on passivity may carry potential risks, as discussed in detail in [17].

III. Proposed Extended Frequency-Domain Passivity Theory

A. Extended Passivity Theory and Extended Definitions of Passivity Index

First, we aim to extend the definitions of the IFP index and the OFP index. To differentiate from those in (1) and (2), the definitions therein are referred to as conventional passivity indices, while the proposed definitions are denoted as extended passivity indices.

Here, definitions of the extended passivity indices are provided: for a MIMO system $\mathbf{G}$, its extended IFP index at frequency ω, denoted as $\nu_R[\mathbf{G}(s),\omega]$, is defined as

$$\frac{1}{2}\min\lambda\left[\mathbf{R}^H(\omega)\,\mathbf{G}(j\omega)+\mathbf{G}^H(j\omega)\,\mathbf{R}(\omega)\right] \tag{6}$$

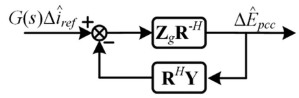

Fig. 7. Interconnected feedback system [$\mathbf{Z}_g\mathbf{R}^{-H}$, $\mathbf{R}^H\mathbf{Y}$].

and the extended OFP index at frequency ω, denoted as $\rho_R[\mathbf{G}(s),\omega]$, is defined as

$$\frac{1}{2}\min\lambda\left[\mathbf{R}^H(\omega)\,\mathbf{G}^{-1}(j\omega)+\mathbf{G}^{-H}(j\omega)\,\mathbf{R}(\omega)\right] \tag{7}$$

where the matrix $\mathbf{R}(\omega)$ is used to weight the system $\mathbf{G}$. The subscript "R" indicates that the extended definition of the indices depends on the weighting matrix $\mathbf{R}(\omega)$.

Based on the extended passivity index definitions in (6) and (7), for the system $[\mathbf{Y},\mathbf{Z}_g]$ of interest, the following result is in order. The proof is given in the Appendix.

Theorem 1: Given stable $\mathbf{Y}$ and exponentially stable and minimum-phase passive $\mathbf{Z}_g$, if there exists $\mathbf{R}$ such that $\forall\omega\geq 0$ for which $j\omega$ is not a pole of $\mathbf{Y}$

$$\nu_R\left[\mathbf{Y}(s),\omega\right]+\rho_R\left[\mathbf{Z}_g(s),\omega\right]>0 \tag{8}$$

and $\forall\omega_0\geq 0$ for which $j\omega_0$ is a pole of $\mathbf{Y}$

$$\rho_R\left[\mathbf{Z}_g(s),\omega_0\right]>0 \tag{9}$$

and

$$\mathbf{R}(\omega_0)^H\mathbf{N}+\mathbf{N}^H\mathbf{R}(\omega_0)\geq 0 \tag{10}$$

where

$$\mathbf{N}:=\lim_{s\to j\omega_0}(s-j\omega_0)\mathbf{Y}(s)$$

then the feedback system is exponentially stable.

Fig. 7 illustrates the idea of the proposed extension, which is similar to the loop transformation performed in [27] for the small gain theory. According to (1) and (2), it is easy to obtain

$$\nu_R\left[\mathbf{Y}(s),\omega\right]=\nu_F\left[\mathbf{R}^H(\omega)\,\mathbf{Y}(s),\omega\right] \tag{11}$$

$$\rho_R\left[\mathbf{Z}_g(s),\omega\right]=\rho_F\left[\mathbf{Z}_g\mathbf{R}^{-H}(s),\omega\right]. \tag{12}$$

When the stability condition in (8) is applied, it is equivalent to assess the stability of the system shown in Fig. 7. The main idea is to prove that the stability of the system in Fig. 7 is equivalent to the stability of the system shown in Fig. 6(b).

Remark 1: Alternatives of the definitions in (6) and (7) may be used to increase the flexibility in choosing the weighting matrix. Specifically, due to the symmetry of an interconnected feedback system, Theorem 1 continues to hold if $\nu_R[\mathbf{G}(s),\omega]$ is replaced by

$$\frac{1}{2}\min\lambda\left[\mathbf{G}(j\omega)\,\mathbf{R}^H(\omega)+\mathbf{R}(\omega)\,\mathbf{G}^H(j\omega)\right] \tag{13}$$

and $\rho_R[\mathbf{G}(s),\omega]$ by

$$\frac{1}{2}\min\lambda\left[\mathbf{G}^{-1}(j\omega)\,\mathbf{R}^H(\omega)+\mathbf{R}(\omega)\,\mathbf{G}^{-H}(j\omega)\right]. \tag{14}$$

It should be noted that the stability condition in Theorem 1 is a sufficient condition for the system stability. While it might be possible to obtain necessary and sufficient conditions for

robust feedback stability in Theorem 1 using the methods in [28], [29], [30], [31], these conditions would revert to the standard passivity and hence of limited relevance to the inverter application considered in this work for the following reason. Since the grid-connected inverter is user designed, the uncertainty in the feedback system lies within the grid itself, which is known to be passive. Robust stability against passive uncertain necessitates the inverter to be strictly passive, which is infeasible in practice as discussed in [17].

B. Implementation Guideline: Using Different Weight Matrices Across Different Frequency Bands

The matrix $\mathbf{R}$ introduces an additional degree of freedom in the definition of the passivity index. The selection of $\mathbf{R}$ can be either frequency-dependent or constant, which gives rise to different reshaping of the dynamics of the inverter and the grid. When the matrix $\mathbf{R}$ is the identity matrix, the extended IFP index, OFP index, and the corresponding stability conditions are consistent with the conventional passivity theory. In [12] and [16], it has been demonstrated that the inherent nondissipative characteristic of grid-connected inverters mainly occurs around $\omega = 0$. At higher frequencies, conventional passivity theory can effectively analyze grid–inverter interactions, assess system stability, and guide control design. Therefore, it is sufficient to find an appropriate weighting matrix $\mathbf{R}$ that can satisfy the conditions in (8) in the low-frequency range of interest.

Assuming that in the low-frequency range $[0, \omega_L)$, (4) does not hold, while it holds in the high-frequency range $[\omega_L, \infty]$. Then, $[0, \omega_L)$ is the frequency range of interest, where ω_L generally does not exceed 2.0 p.u. [3]. In this case, the objective is to identify a suitable matrix $\mathbf{R}(\omega)$ for $\omega \in [0, \omega_L)$. The frequency range $[0, \omega_L]$ can be further discretized into several segments, for instance, $[0, 0.5\omega_L]$ and $(0.5\omega_L, \omega_L)$. Concerning the selection of $\mathbf{R}$, an numerical choice can be made using the convex optimization toolbox (e.g., CVX) in MATLAB. Opt for $\mathbf{R}(0.25\omega_L)$ and $\mathbf{R}(0.75\omega_L)$ such that (8) hold at $\omega = 0.25\omega_L$ and $\omega = 0.75\omega_L$. Subsequently, set $\mathbf{R}(\omega) = \mathbf{R}(0.25\omega_L)$ for $\omega \in [0, 0.5\omega_L]$ and $\mathbf{R}(\omega) = \mathbf{R}(0.75\omega_L)$ for $\omega \in (0.5\omega_L, \omega_L)$ and verify the satisfaction of condition in (8) for all $\omega \in [0, \omega_L)$. If it is met, the process is complete. Otherwise, consider using finer frequency segments, and repeat the same procedure. The process has been summarized as a flow chart, as shown in Fig. 8. However, it is important to note that the purpose of this part is merely to provide a possible approach for finding the weighting matrix, and it does not guarantee that a suitable weighting matrix necessarily exists. Besides numerical methods, analytical or trial-and-error approaches may also be used to identify a potentially suitable weighting matrix.

IV. Rotated Passivity Index and Corresponding Sufficient Stability Condition

When applying passivity theory to grid-connected inverter systems, it is typically desired that passivity theory provides a means for dynamic specification and inverter control design guidelines. Therefore, rather than investigating whether a weighting matrix exists for a specific grid-connected inverter system that satisfies the stability conditions, it is of more interest to propose a fixed weighting matrix and frequency band selection that can serve as a specification guideline for inverter control design as well as stability specification.

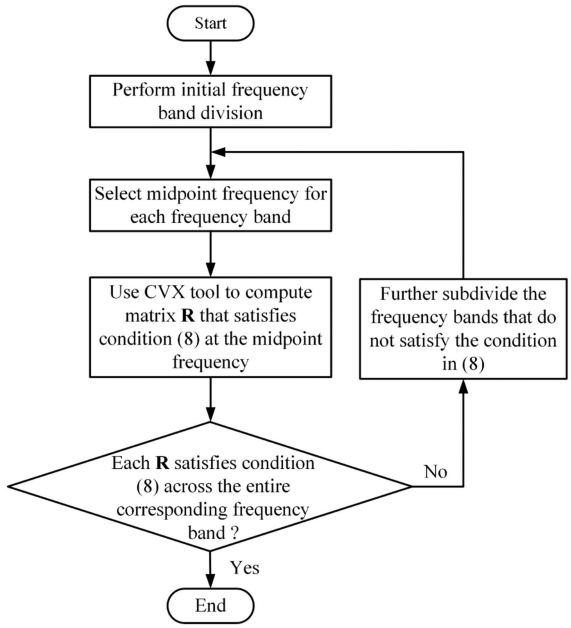

Fig. 8. Flow chart of using CVX tool to find suitable weighting matrix.

Thus, in this section, we aim to provide a fixed, simple selection for the weighting matrix $\mathbf{R}$ and the frequency band division (the choice of ω_L) between the extended passivity theory and the conventional passivity theory. To avoid any confusion, it needs to be repeated that in the subsequent context, the IFP index of $\mathbf{R}^H\mathbf{Y}$ refers to the extended IFP index of $\mathbf{Y}$. Similarly, the OFP index of $\mathbf{Z}_g\mathbf{R}^{-H}$ refers to the extended OFP index of $\mathbf{Z}_g$.

A. Selecting Rotation Matrix as Weighting Matrix

First, set

$$\mathbf{R} = \begin{bmatrix} \cos\left(\frac{\pi}{2}\right) & \sin\left(\frac{\pi}{2}\right) \\ -\sin\left(\frac{\pi}{2}\right) & \cos\left(\frac{\pi}{2}\right) \end{bmatrix} = \begin{bmatrix} 0 & 1 \\ -1 & 0 \end{bmatrix} \tag{15}$$

which is a rotation matrix corresponding to the complex number -*j*. When applied to a matrix, it swaps the diagonal elements with the off-diagonal elements. According to (6) and (7), the inverter admittance $\mathbf{Y}$ and the grid impedance $\mathbf{Z}_g$ are weighted by the left multiplication of matrix $\mathbf{R}^H$ and the right multiplication of $\mathbf{R}^{-H}$, respectively. The inverter admittance and grid impedance matrix is given as

$$\mathbf{Y} = \begin{bmatrix} Y_{11} & Y_{12} \\ Y_{21} & Y_{22} \end{bmatrix}, \quad \mathbf{Z}_g = \begin{bmatrix} sL_g & -\omega_1 L_g \\ \omega_1 L_g & sL_g \end{bmatrix}. \tag{16}$$

In this work, the extended passivity index obtained using a rotation matrix as the weighting matrix is referred to as the *rotated passivity index*. By substituting (15) and $\mathbf{Y}$ from (16) into (6), the rotated IFP index of $\mathbf{Y}$ is obtained. Similarly, by substituting (15) and $\mathbf{Z}_g$ from (16) into (7), the rotated OFP index of $\mathbf{Z}_g$ is obtained. Specifically, inverter admittance after

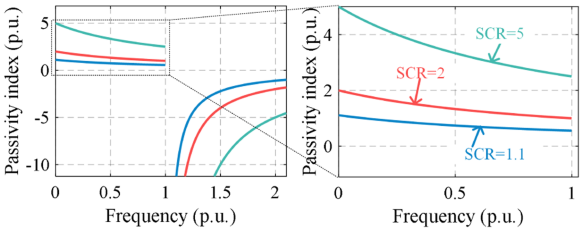

Fig. 9. Plot of the proposed extended OFP index of grid impedance under different SCRs.

being weighted is given as

$$\mathbf{R}^H\mathbf{Y} = \begin{bmatrix} -Y_{21} & -Y_{22} \\ Y_{11} & Y_{12} \end{bmatrix}. \tag{17}$$

Grid impedance $\mathbf{Z}_g$ after being weighted is given as

$$\mathbf{Z}_g\mathbf{R}^{-H} = \begin{bmatrix} \omega_1 L_g & sL_g \\ -sL_g & \omega_1 L_g \end{bmatrix}. \tag{18}$$

Since the $\mathbf{Z}_g$ is a passive component, according to [32], it is straightforward to transform its matrix form in (16) into a complex vector form containing real and imaginary parts. In (16), before the grid impedance is weighted, the term $\omega_1 L_g$ is in the imaginary part and does not contribute any excess passivity. However, after being weighted, $\omega_1 L_g$ moves to the real part, as shown in (18). Define the short-circuit ratio (SCR) as the reciprocal of the per-unit (p.u.) value of L_g. The OFP index plot of $\mathbf{Z}_g\mathbf{R}^{-H}$ with different SCRs is given in Fig. 9. The frequency on the horizontal axis is also in p.u., with the base value ω_b set to $50 \times 2\pi$ rad/s. Since the base frequency is the same as the operating frequency of the grid, denoted as ω_1, we have $\omega_1 = 1.0$ p.u.

B. Frequency Band Separation Between Rotated Passivity Index and Conventional Passivity Index

When discussing the frequency band division between the rotated passivity index and the conventional passivity index, it is necessary to consider the applicable frequency ranges of the stability conditions corresponding to both the proposed rotated passivity index and the conventional passivity index.

First, the applicable frequency range for the stability conditions after selecting the rotated passivity index is discussed. The extended OFP index of $\mathbf{Z}_g$ after being weighted (or equivalently, the OFP index of $\mathbf{Z}_g\mathbf{R}^{-H}$) is positive in $[0, \omega_1)$ and becomes negative when the frequency is higher than ω_1. Furthermore, the rotated IFP index of the inverter admittance is likely negative across the entire frequency range (details will be presented in the next two Sections). Consequently, the stability condition in (8) cannot be satisfied at frequencies greater than ω_1 if $\mathbf{R}$ is configured as in (15). The applicable frequency range for the stability conditions corresponding to the rotated passivity index is denoted as $[0, \omega_L)$, where $\omega_L \leq \omega_1$, as shown in Fig. 10(a). Next, the applicable frequency range for the conventional passivity-based stability condition is considered, denoted as $[\omega_C, \infty]$, as shown in Fig. 10(b). Generally, the choice of ω_C is flexible. However, to ensure that both stability conditions cover the entire frequency range, the relationship between the frequencies should satisfy $\omega_C \leq \omega_L \leq \omega_1$, as illustrated in Fig. 10(c). It should be emphasized again that this requirement applies when dividing the frequency bands; once these three frequencies are fixed, inverter control designs that meet this standard can then be sought.

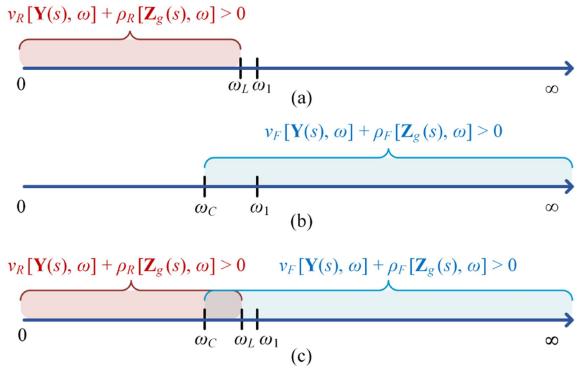

Fig. 10. Illustration of frequency band division. (a) Frequency range applicable to the stability conditions corresponding to the rotated passivity index. (b) Frequency range applicable to the stability conditions corresponding to the conventional passivity index. (c) Combined stability conditions across the entire frequency range.

C. Rotated Passivity Index-Based Stability Condition

The stability condition shown in Fig. 10(c) can be summarized as follows:

1) For frequencies in the range $\omega \in [0, \omega_L)$, the matrix $\mathbf{R}$ is selected according to (15) to ensure that the passivity index of the grid impedance and inverter admittance, weighted by $\mathbf{R}$, satisfies (8).
2) For frequencies in the range $[\omega_C, \infty]$, $\mathbf{R}$ is chosen as the identity matrix, representing conventional passivity indices, with the condition that $\omega_C \leq \omega_L$. If the conditions in (5) are satisfied in this interval, the feedback system is stable.

In the following sections, this sufficient condition for system stability will be employed to analyze grid-inverter interactions and guide inverter control design. It should be noted that in all the numerical example presented later, $\omega_c = \omega_L = \omega_1 = 1.0$ p.u.

V. Applications in PLL-Synchronized Inverters

A. Dissipative Characteristics Analysis of PLL-Synchronized Inverters

In the case of a PLL-synchronized inverter, its input admittance expression, excluding time delay, is given by

$$Y_{dd} = \frac{R_a}{sL + R_a} G_{ad} + \frac{1}{sL + R_a} \frac{s}{s + \alpha_f}$$

$$Y_{qd} = \frac{R_a}{sL + R_a} \frac{i_{q0}}{E_0} \frac{\alpha_p}{s + \alpha_p}$$

$$Y_{dq} = -\frac{R_a}{sL + R_a} \frac{K_v}{s}$$

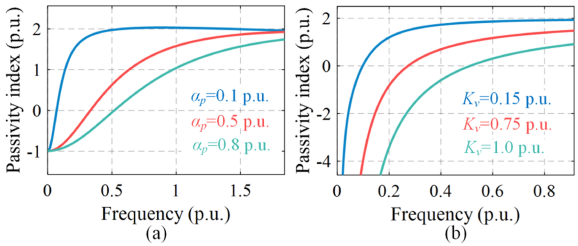

Fig. 11. Plots of the conventional IFP index of a PLL-synchronized inverter with (a) different PLL bandwidths and (b) different AVC gains.

TABLE I
PARAMETERS OF CASE 1-CASE 4IN P.U

Parameters	Case 1	Case 2	Parameters	Case 3	Case 4
L	0.08	0.08	L	0.08	0.08
L_g	0.92	0.92	L_g	0.1	0.9
P	1.0	1.0	P	1.0	1.0
α_c	8	8	α_c	8	8
α_p	1.3	1.3	α_a	0.05	0.05
α_{aq}	0.1	1.3	α_f	15	15
α_f	15	15	G_{ad}	7.5	1.2
G_{ad}	0.45	1.2	G_{aq}	7.5	1.2
G_{aq}	2.25	2.25	K_v	0	0.75
K_v	0.75	0.75			

$$Y_{qq} = \frac{R_a}{sL + R_a}\left(G_{aq}\frac{s}{s+\alpha_p} - \frac{i_{d0}}{E_0}\frac{\alpha_p}{s+\alpha_p}\right) + \frac{1}{sL+R_a}\left(\frac{s}{s+\alpha_f}\frac{s}{s+\alpha_p}\right). \tag{19}$$

This admittance model encompasses CC, PLL, and AVC, with RPC disabled. First, a case with CC loop and PLL is considered. In this scenario, Y_{dq} is 0, and the inverter's nondissipative region is primarily caused by the PLL. Fig. 11(a) shows the variation of the passivity index of the inverter with different PLL bandwidths. The remaining parameters are set as follows: the α_c is 8 p.u., L is 0.08 p.u., P is 1.0 p.u., and Q is 0.1 p.u. When AVC is activated, the integrator in the AVC will dominate in the low-frequency range. The conventional IFP index plots of the inverter admittance for different K_v values are shown in Fig. 11(b). It can be observed that with an increase in PLL bandwidth and voltage control gain, the negative frequency region of the index widens.

B. Numerical Examples of Proposed Rotated Passivity Indices

Cases 1 and 2 are the numerical examples of PLL-synchronized inverters, where the parameters are given in Table I. For Case 1, the system exhibits low-frequency oscillations at the frequency of 0.64 p.u., as shown in Fig. 12(a). In Fig. 12(b), the plot of the conventional IFP index of $\mathbf{Y}$ is shown. In Fig. 12(c), the plots of the extended IFP index of $\mathbf{Y}$ (repeated for clarification, the IFP index of $\{\mathbf{R}^H\mathbf{Y}\}$) and the extended OFP index of $\mathbf{Z}_g$ (the OFP index of $\{\mathbf{Z}_g\mathbf{R}^{-H}\}$) are given. Since the closed-loop system is unstable, both the conventional passivity-based and the extended passivity-based stability conditions are not met.

For Case 2, the q-axis active damping (AD) method proposed in [33] is employed, with the gain α_{aq} adjusted to match the bandwidth of the PLL. However, the conventional IFP index plot

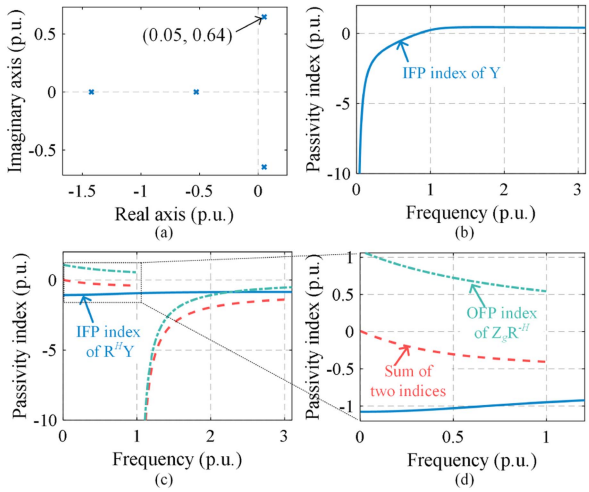

Fig. 12. Numerical example of Case 1. (a) Pole map of the closed-loop system. (b) Conventional IFP index of $\mathbf{Y}$. (c) Proposed rotated passivity index plots, IFP index of $\mathbf{R}^H\mathbf{Y}$(solid), OFP index of $\mathbf{Z}_g\mathbf{R}^{-H}$(dashed-dotted), and IFP index of $\mathbf{R}^H\mathbf{Y}$+OFP index of $\mathbf{Z}_g\mathbf{R}^{-H}$(dashed). (d) Zooming.

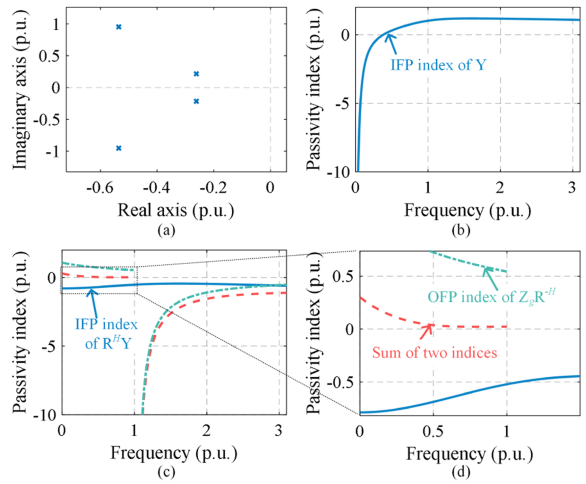

Fig. 13. Numerical example of Case 2. (a) Pole map of the closed-loop system. (b) Conventional IFP index of $\mathbf{Y}$. (c) Proposed rotated passivity index plots, IFP index of $\mathbf{R}^H\mathbf{Y}$(solid), OFP index of $\mathbf{Z}_g\mathbf{R}^{-H}$(dashed-dotted), and IFP index of $\mathbf{R}^H\mathbf{Y}$+OFP index of $\mathbf{Z}_g\mathbf{R}^{-H}$(dashed). (d) Zooming.

of $\mathbf{Y}$, as shown in Fig. 13(b), presents limited insights. It is only confirmed that the condition in (4) is satisfied when $\omega \geq 0.5$ p.u. For $\omega \in [0, 0.5]$ p.u., negative IFP index values are yielded. Since the conventional passivity-based stability condition is not upheld across all frequencies, comprehensive stability specifications for the system cannot be provided in Fig. 13(b). In Fig. 13(c), the plots of the extended IFP index of $\mathbf{Y}$ and the extended OFP index of $\mathbf{Z}_g$ are given. The condition in (8) holds when $\omega \in [0, 1]$ p.u. The condition for the system stability based on the rotated passivity index proposed in Section IV is met, indicating system stability. The system root plot in Fig. 13(a) further confirms this conclusion.

VI. APPLICATIONS IN PC-SYNCHRONIZED INVERTERS

The article takes the PSC control with inner loops of vector current and vector voltage control as an example. The parameter

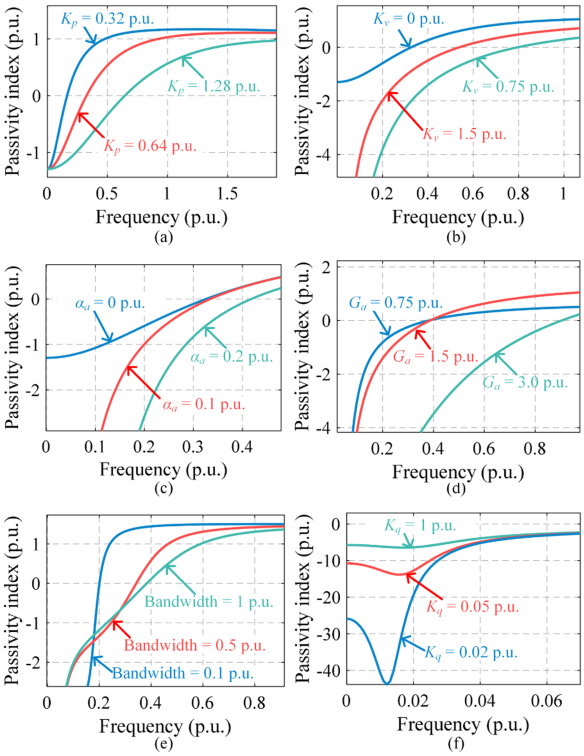

Fig. 14. Plots of the conventional IFP index of a PC-synchronized inverter with (a) different PC gains, (b) different *d-q* AVC gains, (c) different *d-d* and *q-q* AVC integral gains, (d) different *d-d* and *q-q* AVC proportional gains, (e) different LPF bandwidths in the active PC, and (f) different *Q–V* droop gains (K_q).

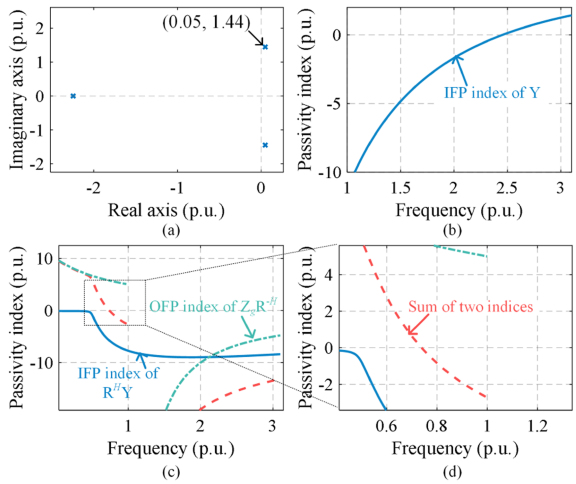

Fig. 15. Numerical example of Case 3. (a) Pole map of the closed-loop system. (b) Conventional IFP index of $\mathbf{Y}$. (c) Proposed rotated passivity index plots, IFP index of $\mathbf{R}^H\mathbf{Y}$(solid), OFP index of $\mathbf{Z}_g\mathbf{R}^{-H}$(dashed-dotted), and IFP index of $\mathbf{R}^H\mathbf{Y}$+OFP index of $\mathbf{Z}_g\mathbf{R}^{-H}$(dashed). (d) Zooming.

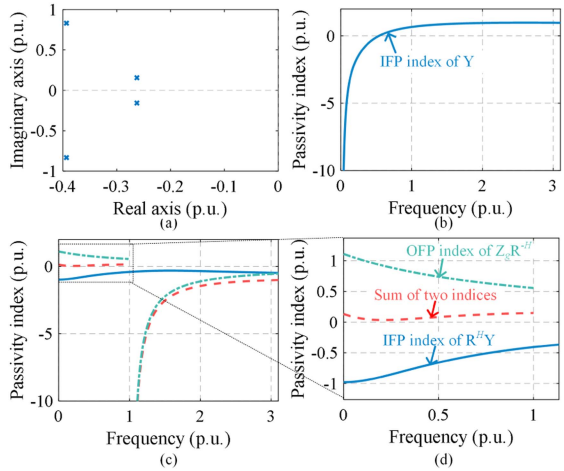

Fig. 16. Numerical example of Case 4. (a) Pole map of the closed-loop system. (b) Conventional IFP index of $\mathbf{Y}$. (c) Proposed rotated passivity index plots, IFP index of $\mathbf{R}^H\mathbf{Y}$(solid), OFP index of $\mathbf{Z}_g\mathbf{R}^{-H}$(dashed-dotted), and IFP index of $\mathbf{R}^H\mathbf{Y}$+OFP index of $\mathbf{Z}_g\mathbf{R}^{-H}$(dashed). (d) Zooming.

design follows the guidelines in [20], with the current controller being a proportional controller with a gain of R_a. The voltage control employs a proportional-integral controller, and to ensure an adequate stability margin, the integral gain is usually set relatively small [20].

Fig. 14 illustrates the relationship between the conventional IFP index of $\mathbf{Y}$ and different control parameters. The impact of the proportional gain of PC, the asymmetric *d-q* damping used in [34], the integral gain in the vector voltage control, the proportional gain in the vector voltage control, the bandwidth of the low pass filter in PC, and the RPC gain K_q (*Q–V* droop gain) on the conventional IFP index plots are shown in Fig. 14(a)–(f), respectively. Generally, reducing the gain of the active power controller, narrowing the bandwidth of the low-pass filter in the active PC, lowering the voltage control gain, or increasing the *Q–V* droop control gain can enhance the passivity degree of the inverter. However, the nondissipative characteristic of the inverter at low frequencies remains unchanged. The analysis of PC-synchronized inverters at low frequencies based on traditional passivity theory has been discussed in detail in [12]. Hence, this article will not elaborate further on this topic.

Two numerical examples of PC-synchronized inverters are given here, which are denoted as Case 3, and Case 4. The parameters are given in Table I. Case 3 presents an unstable example, as shown in Fig. 15(a). The conventional passivity index plot and proposed passivity index without considering α_a are given in Fig. 15(b) and (c), respectively. Due to the instability of the closed-loop system, it is easily discernible from the plot of the passivity index that the system does not satisfy the stability conditions. Although the method proposed cannot directly predict instability, the stability assessment approach presented in Section IV-C provides valuable insights for system diagnostics and inverter adjustment when the stability conditions are not met. From the passivity index plots in Fig. 15(b) and (c), it is evident that the oscillation frequency fall within the range, where the stability conditions in Section IV-C are not satisfied. Therefore, the proposed method can also serve as an indicator of risky frequency band.

Case 4 is a stable example, the *d-q* integral-based control is considered here. This inclusion causes the conventional IFP index of $\mathbf{Y}$ to become negative infinity at $\omega = 0$, as shown in Fig. 16(b). Similar to the cases of the PLL-synchronized inverters, the conventional passivity-based stability condition in (4) cannot hold for ω below 0.6 p.u. However, with the proposed rotated passivity index, as shown in Fig. 16(c), (8) holds for

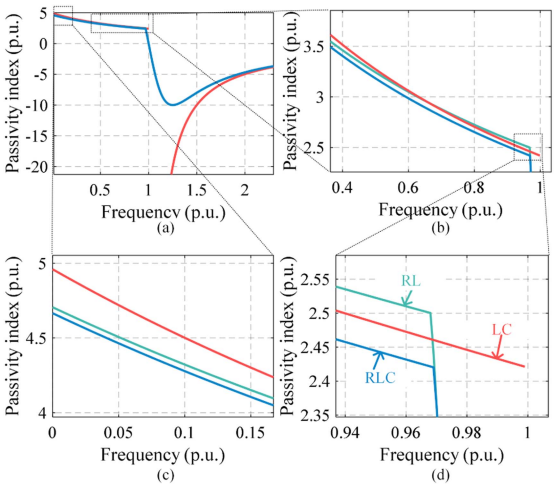

Fig. 17. (a) Extended OFP index of different types of grid impedance. (b) Zooming. (c) Zooming. (d) Zooming.

$\omega \in [0, 1)$ p.u. By selecting ω_L as 1.0 p.u., the condition for the system stability based on the rotated passivity index proposed in Section IV is met, indicating system stability. The system root plot in Fig. 16(a) further confirms this conclusion.

VII. Discussion

This section provides a detailed discussion of the proposed method, focusing on three main aspects. First, it addresses the sources and impacts of uncertainty in the system and how the proposed method can be applied for robust inverter control design. Second, a comparison is made with other multivariable theories, primarily from the perspectives of complexity and conservativeness. Third, the compatibility of the proposed method with SISO systems and its limitations are discussed.

A. Sources and Impacts of Uncertainty in the System

In this work, the inverter model (including the control structures and parameters) is user-defined and adjustable, but the grid impedance is variable due to the inherent complexity of the power grid [1]. For the system of interest, the source of uncertainty comes from the grid impedance, particularly its type and the value of grid inductance, i.e., SCR [35]. In this study, it is assumed that the low-frequency grid impedance is purely inductive. However, in practice, grid impedance may be RL, RC, or RLC. In Fig. 17, when $L_g = 0.2$ p.u. (corresponding to $SCR = 5$ in Fig. 9), the rotated OFP index for different types of grid impedance is plotted, where $R = 0.05$ p.u. and $C = 0.04$ p.u., with the values of R and C based on the practical setup referenced in [20]. From the zoomed-in views of Fig. 17(b)–(d), it can be observed that at low frequencies, the impact of resistance and capacitance on the rotated passivity index is minimal, with a difference of only around 0.3 in the maximum values and a narrow applicable frequency range difference of merely 0.03 p.u. Therefore, the uncertainty in the type of grid impedance does not significantly affect the proposed method, as long as it remains inductance-dominated.

On the other hand, the magnitude of the grid inductance uncertainty (SCR) has a significant impact, as demonstrated in Fig. 10. The rotated OFP index of the grid impedance varies greatly under different SCRs. As indicated by (8), the excessive OFP index value of the grid impedance at low frequencies is a critical reference for adjusting the inverter design. When the SCR is known, directly applying the condition in (8) is straightforward. However, when the information of grid impedance is unknown, ensuring that the inverter design remains robust against variations in SCR is a common challenge [35].

Here, we propose a simple yet effective robust design approach against SCR uncertainties. When applying a rotation matrix to weight the grid impedance, as shown in Fig. 9, it is observed that as SCR increases, the surplus passivity provided by the grid impedance at low frequencies also increases. In practical systems, SCR $= 1.1$ is almost the lowest SCR that might be encountered [1]. Therefore, when designing the inverter, replacing the actual L_g in (8) with 0.9 p.u. ($SCR = 1.1$) will yield a design that is robust to SCR variations. As long as the actual SCR exceeds 1.1, the closed-loop system remains stable.

B. Comparison With Other Multivariable Techniques

As shown in Fig. 10, the contribution of this work is to propose a new passivity-based stability condition for the low-frequency range, building upon the conventional passivity-based stability criterion. This results in a stability condition that spans the entire frequency range, applicable to grid-connected inverter systems. Based on other multivariable control theories, such as small-gain [36] and small-phase [37] theories, low-frequency stability conditions also exist as a complement to Fig. 10(b). In the following, these approaches are compared and discussed in terms of complexity and conservativeness.

1) Complexity: Small-phase theory shows promise but remains relatively unfamiliar to the power electronics field [38]. It has a high theoretical threshold and cannot be directly applied to low-frequency grid-connected inverter systems because inverters do not satisfy the sectoriality condition [36], [37]. Extending small-phase theory to this context would require further research, as mentioned in [37]. As for *small-gain theory*, while it can be directly applied to grid-connected inverter systems, it is also known to be quite conservative [39], [40], especially when there exits a pole close to or at the origin in the inverter. Similar to this work, appropriate weighting functions need to be selected to achieve the specified control objectives [36]. *Structured-singular-value theory* is a powerful tool for multivariable control, particularly in addressing robustness in systems with uncertainties. However, it is a generalization of the small-gain theory that suffers from the same drawback in that it is only applicable to open-loop exponentially stable systems and is inapplicable to marginally stable systems with poles on the imaginary axis. Moreover, it introduces additional complexity.

The stability condition proposed in Fig. 10(a) remains within the passivity theory framework and is similar in application to the conventional passivity-based method, making it accessible to those already familiar with passivity theory. Moreover, the approach presented in Section IV employs fixed constant weighting matrices and frequency ranges, eliminating the need

for case-by-case selection of weighting matrices or frequency band divisions. This further enhances its practicality for real-world applications.

2) Conservativeness: When using low-frequency stability conditions based on other theories as a complement to Fig. 10(b), the applicable frequency range becomes a crucial metric. Only when the new stability condition covers a wider frequency range can it be possible to combined with traditional passivity-based stability conditions to derive a stability condition that spans the entire frequency range, as illustrated in Fig. 10(c). If the new stability condition applies to only a narrow frequency range, condition (5) must hold over a broader frequency range. Since small-phase theory still needs further development in the field of power electronics for low frequency region, the comparison is primarily focus on small-gain theory in [36] and the method proposed in this work.

As demonstrated in the examples from the previous sections, the maximum frequency range applicable to the proposed method is $[0, 1]$ p.u., which is sufficient for condition (5) to overlap and cover the entire frequency range. However, according to [36], the applicability of the stability condition based on small-gain theory is case-specific, typically around or below 0.5 p.u. When PC-synchronized inverters are present in the system, the upper frequency limit is further reduced. This implies that condition (5) needs to be satisfied at even lower frequencies, which may result in more conservative design.

It should be noted that decentralized stability conditions capable of covering the entire frequency range can also be obtained in [36], [37]. However, within the framework of the problem addressed here, any method outside of passivity theory would require the simultaneous use of two different theories for stability assessment or inverter design guidance, significantly increasing practical complexity. In contrast, the proposed method is notably simple, striking a balance between theoretical complexity, practical ease of use, and effectiveness.

C. Compatibility With SISO Systems and Limitations

Although all the methods and conclusions in this work are based on MIMO systems, they are still applicable to SISO systems, as a SISO system can be considered a simplified version of a MIMO system. When the system is a SISO transfer function, the passivity index reduces to the real part of the transfer function. It is noteworthy that a fundamental limitation of the proposed theory based on passivity is its inability to handle systems with repeated poles on the imaginary axis. This issue is also present in standard passivity theory [41] and carries over to the extension considered in this article.

VIII. Experimental Results

Experimental tests are conducted for both PLL-synchronized and PC-synchronized inverters. The experimental platform is shown in Fig. 18, and the system and controller parameters are listed in Table II.

Fig. 19(a) presents a stable design for a PLL-synchronized inverter under weak grid conditions. The plots for both the conventional passivity index and the extended passivity index are shown in Fig. 19(b) and (c), respectively. While Fig. 19(b) alone does not provide sufficient information on the system stability, it is evident from Fig. 19(c) that the system satisfies the stability conditions based on the extended passivity index, confirming the system stability.

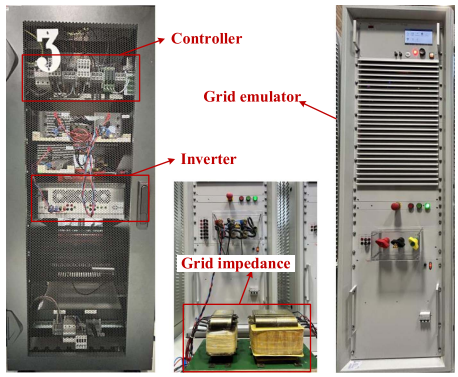

Fig. 18. Experimental platform.

TABLE II
PARAMETERS OF THE EXPERIMENTAL PLATFORM AND THE CONTROLLERS

Parameters	*Actual value (p.u.)*
Rated power	2 kVA (1.0)
Rated voltage	110 V (1.0)
Rated current	8.57 A (1.0)
Based impedance	18.15 Ω (1.0)
Filter inductance L	4 mH (0.07)
Filter capacitance C	10 μF (0.06)
Grid impedance L_g	48 mH (0.83)
Fundamental frequency	50 Hz (1.0)
Switching frequency	10k Hz (200)
Bandwidth of CC	1400π rad/s (14.0) / 800π rad/s (8.0)
α_f	800π rad/s (8.0)

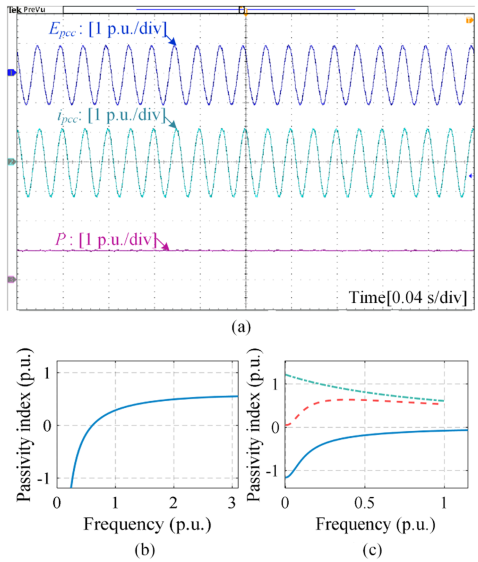

Fig. 19. Stable operation of the PLL-synchronized inverter. (a) Experimental waveform. (b) Conventional IFP index plot of $\mathbf{Y}$. (c) Proposed rotated passivity index plots, IFP index of $\mathbf{R}^H\mathbf{Y}$(solid), OFP index of $\mathbf{Z}_g\mathbf{R}^{-H}$(dashed-dotted), and IFP index of $\mathbf{R}^H\mathbf{Y}$+OFP index of $\mathbf{Z}_g\mathbf{R}^{-H}$(dashed).

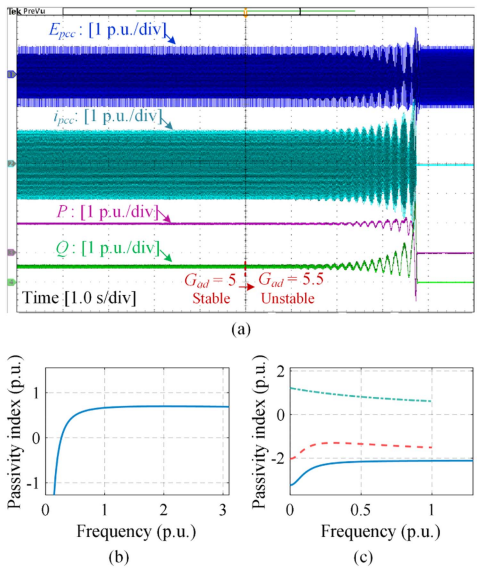

Fig. 20. Unstable operation of the PLL-synchronized inverter with $G_{ad} = 5.5$ p.u. and $G_{aq} = 1$ p.u. (a) Experimental waveform. (b) Conventional IFP index plot of $\mathbf{Y}$. (c) Proposed rotated passivity index plots, IFP index of $\mathbf{R}^H\mathbf{Y}$(solid), OFP index of $\mathbf{Z}_g\mathbf{R}^{-H}$(dashed-dotted), and IFP index of $\mathbf{R}^H\mathbf{Y}$+OFP index of $\mathbf{Z}_g\mathbf{R}^{-H}$(dashed).

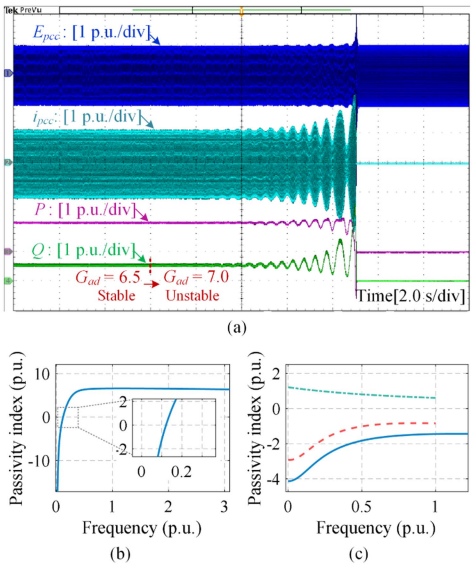

Fig. 21. Unstable operation of the PLL-synchronized inverter with $G_{ad} = 7.0$ p.u. and $G_{aq} = 10$ p.u. (a) Experimental waveform. (b) Conventional IFP index plot of $\mathbf{Y}$. (c) Proposed rotated passivity index plots, IFP index of $\mathbf{R}^H\mathbf{Y}$(solid), OFP index of $\mathbf{Z}_g\mathbf{R}^{-H}$(dashed-dotted), and IFP index of $\mathbf{R}^H\mathbf{Y}$+OFP index of $\mathbf{Z}_g\mathbf{R}^{-H}$(dashed).

In Fig. 20, increasing the gain of the d-axis AD, G_{ad}, leads to low-frequency oscillations, a phenomenon previously reported in [17]. It is clear from Fig. 20(c) that the system fails to satisfy the passivity-based stability conditions, indicating this design is inappropriate compared to the stable design in Fig. 19(c). In Fig. 21, further increasing the AD gain results in even lower-frequency oscillations. However, when comparing Figs. 19(b)–21(b), which show the conventional IFP index of the inverter

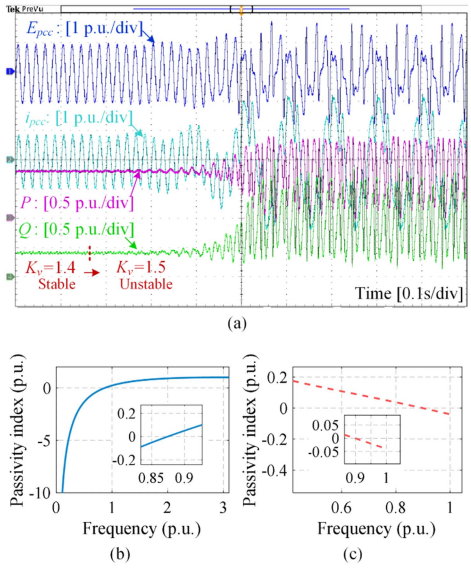

Fig. 22. From stable operation to unstable operation for the PC-synchronized inverter. (a) Experimental waveform. (b) Conventional IFP index plot of $\mathbf{Y}$ of the stable operation. (c) IFP index of $\mathbf{R}^H\mathbf{Y}$+OFP index of $\mathbf{Z}_g\mathbf{R}^{-H}$.

admittance, it is observed that the nondissipative region in the unstable cases of Figs. 20 and 21 is actually narrower than in the stable case. This validates the limitation of the conventional passivity theory in predicting low-frequency stability, as shown again in Fig. 10(b), and also falsifies the common practical recommendation that a narrower nondissipative region correlates with better stability robustness (as discussed in detail in [17]).

It is important to note that the stability conditions proposed in this work are only sufficient conditions for system stability. Thus, our goal is to design the system to meet the conditions shown in Fig. 10(c), ensuring system stability. When the conditions in Fig. 10(c) are not satisfied, the system may be either stable or unstable. Even in this case, checking the rotated passivity index remains valuable because the rotated passivity index plot of the grid impedance provides a clear reference for tuning the inverter index. The index plot clearly indicates which frequency ranges are at risk, allowing targeted adjustments for the inverters.

Fig. 22(a) shows the experimental results of the PC-synchronized inverter under weak grid conditions, showing the system from stability to instability. In Fig. 22(b), the conventional passivity index plot is presented. The system incorporates the asymmetric AD proposed in [34], specifically designed for a strong grid. When the gain of AD is set to 1.0 p.u., by selecting ω_L as 0.9 p.u., it can be observed that the conventional IFP index of $\mathbf{Y}$ is larger than 0 when $\omega \geq \omega_L$ in Fig. 22(b). On the other hand, as shown in Fig. 22(c), IFP index of $\mathbf{R}^H\mathbf{Y}$+OFP index of $\mathbf{Z}_g\mathbf{R}^{-H}$ is larger than 0 when $\omega \leq \omega_L$. Hence, the extended passivity theory-based stability condition is met, and the system is stable. However, as the gain (K_v) is gradually increased, it is observed that the system starts exhibiting negative regions around 1.0 p.u., indicating that excessive gain may lead to instability in this frequency range, as shown in Fig. 23.

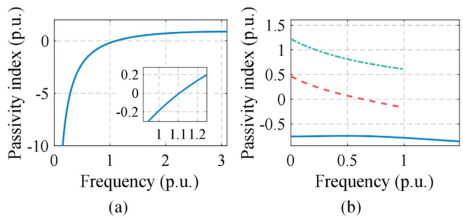

Fig. 23. (a) Conventional IFP index plot of $\mathbf{Y}$ of the unstable operation in Fig. 22. (b) Proposed rotated passivity index plots of the unstable operation in Fig. 22, IFP index of $\mathbf{R}^H\mathbf{Y}$(solid), OFP index of $\mathbf{Z}_g\mathbf{R}^{-H}$(dashed-dotted), and IFP index of $\mathbf{R}^H\mathbf{Y}$+OFP index of $\mathbf{Z}_g\mathbf{R}^{-H}$(dashed).

Continuing to increase K_v results in system instability around 1.0 p.u., as shown in Fig. 22(a).

IX. Conclusion

An extended frequency domain passivity theory is developed in this article, to address the limitations of conventional passivity theory in providing stability and control design specifications for grid-connected inverter systems, particularly at low frequencies. Based on this extended theory, a new passivity index is derived. Numerical and experimental results validate the effectiveness of the new passivity index. Future directions could involve exploring design-oriented studies on the dynamic characteristics of inverters, including dc-side dynamics, within the framework of the rotated passivity index. This might also include investigating appropriate selections for the weighting matrix $\mathbf{R}$ under diverse grid conditions and various inverter control structures. Alternatively, it could entail examining the integration of novel control theories recently developed in [42], [43], [44], [45] with passivity theory in grid-connected inverter systems.

Appendix

First, consider the case where $\mathbf{Y}$ is exponentially stable. According to the definitions in (6) and (7), the extended OFP index of $\mathbf{Z}_g$ and extended IFP index of $\mathbf{Y}$ are obtained as

$$\nu_R\left[\mathbf{Y}(s),\omega\right] \triangleq \frac{1}{2}\min\lambda\left[\mathbf{R}^H(\omega)\,\mathbf{Y}(j\omega)+\mathbf{Y}^H(j\omega)\,\mathbf{R}(\omega)\right] \tag{20}$$

$$\rho_R\left[\mathbf{Z}_g(s),\omega\right] \triangleq \frac{1}{2}\min\lambda\left[\mathbf{R}^H(\omega)\,\mathbf{Z}_g^{-1}(j\omega)+\mathbf{Z}_g^{-H}(j\omega)\mathbf{R}(\omega)\right]. \tag{21}$$

For negative feedback interconnected system [$\mathbf{Y}$, $\mathbf{Z}_g$], the stability condition is that $\det[\mathrm{I}+\mathbf{Z}_g(s)\mathbf{Y}(s)]$ has no zeros in the right-half plane (RHP). Since $\mathbf{Y}$ and $\mathbf{Z}_g$ are stable, $\det[\mathrm{I}+\mathbf{Z}_g(s)\mathbf{Y}(s)]$ does not have poles in the RHP. According to the Nyquist criterion for MIMO systems in [46], system stability is equivalent to the Nyquist plot of $\det[\mathrm{I}+\mathbf{Z}_g(s)\mathbf{Y}(s)]$ not encircling the origin. According to [46], one sufficient condition for the Nyquist plot of $\det[\mathrm{I}+\mathbf{Z}_g(s)\mathbf{Y}(s)]$ not encircling the origin is that

$$\det(\mathrm{I}+\tau\mathbf{Y}(j\omega)\mathbf{Z}_g(j\omega))\neq 0,\forall\omega\geq 0,\forall\tau\in[0,1]. \tag{22}$$

According to [47, Corollary 1], by taking

$$\Theta=\begin{bmatrix}-\rho_R\left[\mathbf{Z}_g(s),\omega\right]\mathrm{I} & \mathbf{R}(\omega)^H\\ \mathbf{R}(\omega) & 0\end{bmatrix}$$
$$\nabla^H=\mathbf{Z}_g(j\omega)$$
$$\mathbf{M}^H=-\mathbf{Y}(j\omega) \tag{23}$$

then

$$\begin{pmatrix}\mathbf{I} & \mathbf{M}\end{pmatrix}\Theta\begin{pmatrix}\mathbf{I}\\ \mathbf{M}^H\end{pmatrix} \tag{24}$$

equals to

$$-\mathbf{R}^H(\omega)\,\mathbf{Y}(j\omega)-\mathbf{Y}^H(j\omega)\,\mathbf{R}(\omega)-\rho_R\left[\mathbf{Z}_g(s),\omega\right]\mathbf{I}. \tag{25}$$

Since $-\mathbf{R}^H(\omega)\mathbf{Y}(j\omega)-\mathbf{Y}^H(j\omega)\mathbf{R}(\omega)\leq-\nu_R[\mathbf{Y}(s),\omega]\mathbf{I}$ and $\nu_R[\mathbf{Y}(s),\omega]+\rho_R[\mathbf{Z}_g(s),\omega]>0$, it is easy to get (24) is negative definite. Similarly

$$\begin{pmatrix}\nabla & \mathbf{I}\end{pmatrix}\Theta\begin{pmatrix}\nabla^H\\ \mathbf{I}\end{pmatrix} \tag{26}$$

equals to

$$\mathbf{R}(\omega)\,\mathbf{Z}_g(j\omega)+\mathbf{Z}_g^H(j\omega)\,\mathbf{R}^H(\omega)-\rho_R\left[\mathbf{Z}_g(s),\omega\right]\mathbf{Z}_g^H(j\omega)\,\mathbf{Z}_g(j\omega). \tag{27}$$

According to (21), (26) is positive semidefinite. Since the conditions of [47, Eqs. (6) and (7)] hold, it is obtained that $\det(\mathrm{I}+\mathbf{Y}(j\omega)\mathbf{Z}_\mathrm{g}(j\omega))\neq 0$. Since $\rho_R[\mathbf{Z}_g(s),\omega]\geq 0$, (24) <0 implies that

$$-\mathbf{R}(\omega)^H[\tau\mathbf{Y}(j\omega)]-[\tau\mathbf{Y}(j\omega)]^H\mathbf{R}(\omega)-\rho_R\left[\mathbf{Z}_g(s),\omega\right]\mathbf{I}<0,\quad\forall\tau\in[0,1] \tag{28}$$

which means $\det(\mathrm{I}+\tau\mathbf{Y}(j\omega)\mathbf{Z}_\mathrm{g}(j\omega))\neq 0,\forall\omega\geq 0,\forall\tau\in[0,1]$, then it can be ensured that the Nyquist plot of $\det[\mathrm{I}+\mathbf{Z}_g(s)\mathbf{Y}(s)]$ does not encircle the origin.

Next, suppose $\mathbf{Y}$ is marginally stable and $j\omega_0$ is a pole of $\mathbf{Y}$. Note that the properties of $\mathbf{Z}_g$ and (9) ensure that

$$\mathbf{R}(\omega_0)\mathbf{Z}_g(j\omega_0)+\mathbf{Z}_g(j\omega_0)^H\mathbf{R}(\omega_0)^H>0. \tag{29}$$

Together, (10) and (29) guarantee that $(I+\mathbf{Z}_g\mathbf{Y})^{-1}$ does not have a pole at $j\omega_0$ and the Nyquist plot of $\det[\mathrm{I}+\mathbf{Z}_g(s)\mathbf{Y}(s)]$ along a small semi-circular indentation around $j\omega_0$ into the RHP cannot intersect with $(-\infty,0]$ and hence no encirclement of the origin can happen. For details, see the proof of the main result in [44].

References

[1] X. Wang, M. G. Taul, H. Wu, Y. Liao, F. Blaabjerg, and L. Harnefors, "Grid-synchronization stability of converter-based resources—an overview," *IEEE Open J. Ind. Appl.*, vol. 1, pp. 115–134, 2020.

[2] Q. Peng, Q. Jiang, Y. Yang, T. Liu, H. Wang, and F. Blaabjerg, "On the stability of power electronics-dominated systems: Challenges and potential solutions," *IEEE Trans. Ind. Appl.*, vol. 55, no. 6, pp. 7657–7670, Nov./Dec. 2019.

[3] L. Harnefors, X. Wang, A. G. Yepes, and F. Blaabjerg, "Passivity-based stability assessment of grid-connected VSCs—an overview," *IEEE Trans. Emerg. Sel. Topics Power Electron.*, vol. 4, no. 1, pp. 116–125, Mar. 2015.

[4] G. Wu et al., "Passivity-based stability analysis and generic controller design for grid-forming inverter," *IEEE Trans.Power Electron.*, vol. 38, no. 5, pp. 5832–5843, May 2023.
[5] J. Bao, P. L. Lee, and B. E. Ydstie, *Process Control: The Passive Systems Approach*, London, U.K.: Springer, 2007.
[6] L. Harnefors, X. Wang, S.-F. Chou, M. Bongiorno, M. Hinkkanen, and M. Routimo, "Asymmetric complex-vector models with application to VSC–grid interaction," *IEEE Trans. Emerg. Sel. Topics Power Electron.*, vol. 8, no. 2, pp. 1911–1921, Jun. 2020.
[7] J. Serrano-Delgado, S. Cobreces, M. Rizo, and E. J. Bueno, "Low-order passivity-based robust current control design for grid-tied VSCs," *IEEE Trans.Power Electron.*, vol. 36, no. 10, pp. 11886–11899, Oct. 2021.
[8] L. Harnefors, A. G. Yepes, A. Vidal, and J. Doval-Gandoy, "Passivity-based controller design of grid-connected VSCs for prevention of electrical resonance instability," *IEEE Trans. Ind. Electron.*, vol. 62, no. 2, pp. 702–710, Feb. 2015.
[9] C. Hirsching et al., "Passivity-based sensitivity analysis of the inner current controller in grid-following MMC-HVDC applications - an overview," in *Proc. 46th Annu. Conf. IEEE Ind. Electron. Soc.*, 2020, pp. 1412–1417.
[10] I. Z. Petric, P. Mattavelli, and S. Buso, "Multi-sampled grid-connected VSCs: A path toward inherent admittance passivity," *IEEE Trans.Power Electron.*, vol. 37, no. 7, pp. 7675–7687, Jul. 2022.
[11] X. Lin, Y. Wen, R. Yu, J. Yu, and H. Wen, "Improved weak grids synchronization unit for passivity enhancement of grid-connected inverter," *IEEE Trans. Emerg. Sel. Topics Power Electron.*, vol. 10, no. 6, pp. 7084–7097, Dec. 2022.
[12] F. Zhao, X. Wang, and T. Zhu, "Low-frequency passivity-based analysis and damping of power-synchronization controlled grid-forming inverter," *IEEE Trans. Emerg. Sel. Top. Power Electron.*, vol. 11, no. 2, pp. 1542–1554, Apr. 2023.
[13] L. Harnefors, M. Bongiorno, and S. Lundberg, "Input-admittance calculation and shaping for controlled voltage-source converters," *IEEE Trans. Ind. Electron.*, vol. 54, no. 6, pp. 3323–3334, Dec. 2007.
[14] M. Beza and M. Bongiorno, "Impact of converter control strategy on low-and high-frequency resonance interactions in power-electronic dominated systems," *Int. J. Elect. Power Energy Syst.*, vol. 120, Sep. 2020, Art. no. 105978.
[15] A. J. Agbemuko, J. L. Domínguez-García, O. Gomis-Bellmunt, and L. Harnefors, "Passivity-based analysis and performance enhancement of a vector controlled VSC connected to a weak ac grid," *IEEE Trans. Power Del.*, vol. 36, no. 1, pp. 156–167, Feb. 2021.
[16] F. Chen, L. Zhao, L. Harnefors, J. Kukkola, M. Routimo, and X. Wang, "Pitfalls of using passivity index to guide grid-connected inverter control design in low-frequency region," in *Proc. IEEE Energy Convers. Congr. Expo.*, 2023, pp. 758–764.
[17] F. Chen et al., "Limitations of using passivity index to analyze grid–inverter interactions," *IEEE Trans. Power Electron.*, vol. 39, no. 11, pp. 14465–14477, Nov. 2024.
[18] FINGRID, "Specific study requirements for grid energy storage systems," Jun. 2023. [Online]. Available: https://www.fingrid.fi/globalassets/dokumentit/fi/palvelut/kulutuksen-ja-tuotannon-liittaminen-kantaverkkoon/specific-study-requirements-for-grid-energy-storage-systems-en.pdf
[19] L. Zhang, "Modeling and control of VSC-HVDC links connected to weak ac systems," Ph.D. dissertation, Dept. School Elect. Eng., Stockholm, Sweden, 2011.
[20] L. Harnefors, J. Kukkola, M. Routimo, M. Hinkkanen, and X. Wang, "A universal controller for grid-connected voltage-source converters," *IEEE Trans. Emerg. Sel. Topics Power Electron.*, vol. 9, no. 5, pp. 5761–5770, Oct. 2021.
[21] F. Zhao, X. Wang, and T. Zhu, "Power dynamic decoupling control of grid-forming converter in stiff grid," *IEEE Trans. Power Electron.*, vol. 37, no. 8, pp. 9073–9085, Aug. 2022.
[22] B. Wen, D. Boroyevich, R. Burgos, P. Mattavelli, and Z. Shen, "Analysis of D-Q small-signal impedance of grid-tied inverters," *IEEE Trans.Power Electron.*, vol. 31, no. 1, pp. 675–687, Jan. 2016.
[23] C. Li, J. Liang, L. M. Cipcigan, W. Ming, F. Colas, and X. Guillaud, "DQ impedance stability analysis for the power-controlled grid-connected inverter," *IEEE Trans. Energy Convers.*, vol. 35, no. 4, pp. 1762–1771, Dec. 2020.
[24] P. Moylan and D. Hill, "Stability criteria for large-scale systems," *IEEE Trans. Autom. Control*, vol. 23, no. 2, pp. 143–149, Apr. 1978.
[25] Y. Liao and X. Wang, "Impedance-based stability analysis for interconnected converter systems with open-loop RHP poles," *IEEE Trans.Power Electron.*, vol. 35, no. 4, pp. 4388–4397, Apr. 2020.
[26] M. Beza and M. Bongiorno, "Identification of resonance interactions in offshore-wind farms connected to the main grid by MMC based HVDC system," *Int. J. Elect. Power Energy Syst.*, vol. 111, pp. 101–113, Oct. 2019.
[27] M. Green and D. J. Limebeer, *Linear Robust Control*. North Chelmsford, MA, USA: Courier Corporation, 2012.
[28] S. Z. Khong and A. van der Schaft, "On the converse of the passivity and small-gain theorems for input–output maps," *Automatica*, vol. 97, pp. 58–63, 2018.
[29] S. Z. Khong and C.-Y. Kao, "Converse theorems for integral quadratic constraints," *IEEE Trans. Automat. Control*, vol. 66, no. 8, pp. 3695–3701, Aug. 2021.
[30] S. Z. Khong and C.-Y. Kao, "Addendum to "Converse theorems for integral quadratic constraints," *IEEE Trans. Automat. Control*, vol. 67, no. 1, pp. 539–540, Jan. 2022.
[31] A. Ringh, X. Mao, W. Chen, L. Qiu, and S. Z. Khong, "Gain and phase type multipliers for structured feedback robustness," *IEEE Trans. Autom. Control*, 2024.
[32] L. Harnefors, "Modeling of three-phase dynamic systems using complex transfer functions and transfer matrices," *IEEE Trans. Ind. Electron.*, vol. 54, no. 4, pp. 2239–2248, Aug. 2007.
[33] F. Chen, L. Zhao, L. Harnefors, X. Wang, J. Kukkola, and M. Routimo, "Enhanced Q-axis voltage integral damping control for fast PLL-synchronized inverters in weak grids," *IEEE Trans.Power Electron.*, vol. 39, no. 1, pp. 424–435, Jan. 2024.
[34] F. Chen, L. Zhao, L. Harnefors, J. Kukkola, M. Routimo, and X. Wang, "Dynamics enhancement for power synchronization control with asymmetric ac voltage controller in strong grids," in *Proc. IEEE Conf. Control Technol. Appl.*, 2023, pp. 1066–1070.
[35] L. Harnefors, M. Hinkkanen, U. Riaz, F. M. M. Rahman, and L. Zhang, "Robust analytic design of power-synchronization control," *IEEE Trans. Ind. Electron.*, vol. 66, no. 8, pp. 5923–5933, Aug. 2019.
[36] L. Huang et al., "Gain and phase: Decentralized stability conditions for power electronics-dominated power systems," *IEEE Trans. Power Syst.*, vol. 39, no. 6, pp. 7240–7256, Nov. 2024.
[37] L. Woolcock and R. Schmid, "Mixed gain/phase robustness criterion for structured perturbations with an application to power system stability," *IEEE Control Syst. Lett.*, vol. 7, pp. 3193–3198, 2023.
[38] D. Wang, W. Chen, and L. Qiu, "The first five years of a phase theory for complex systems and networks," *IEEE/CAA J. Autom. Sinica*, vol. 11, no. 8, pp. 1573–1589, Aug. 2024.
[39] Z. Liu, J. Liu, W. Bao, and Y. Zhao, "Infinity-norm of impedance-based stability criterion for three-phase ac distributed power systems with constant power loads," *IEEE Trans. Power Electron.*, vol. 30, no. 6, pp. 3030–3043, Jun. 2015.
[40] Y. Song and C. Breitholtz, "Vsc-hvdc system robust stability analysis based on a modified mixed small gain and passivity theorem," *IFAC-PapersOnLine*, vol. 50, no. 1, pp. 13–18, 2017.
[41] B. D. Anderson and S. Vongpanitlerd, *Network Analysis and Synthesis: A Modern Systems Theory Approach*. North Chelmsford, MA, USA: Courier Corporation, 2013.
[42] W. Chen, D. Wang, S. Z. Khong, and L. Qiu, "A phase theory of multi-input multi-output linear time-invariant systems," *SIAM J. Control Optim.*, vol. 62, no. 2, pp. 1235–1260, 2024.
[43] X. Mao, W. Chen, and L. Qiu, "Phases of discrete-time LTI multivariable systems," *Automatica*, vol. 142, 2022, Art. no. 110311.
[44] S. Z. Khong, "Feedback stability of generalised positive real and negative imaginary systems," *IEEE Trans. Autom. Control*, vol. 68, no. 10, pp. 6285–6290, Oct. 2022.
[45] S. Z. Khong and A. Lanzon, "Feedback stability analysis via frequency dependent constraints," *IEEE Trans. Autom. Control*, early access, Sep. 10, 2024, doi: 10.1109/TAC.2024.3457432.
[46] S. Skogestad and I. Postlethwaite, *Multivariable Feedback Cntrol: Analysis and Design*. New York, USA: John Wiley & Sons, Inc., 2005.
[47] T. Iwasaki and S. Hara, "Well-posedness of feedback systems: Insights into exact robustness analysis and approximate computations," *IEEE Trans. Automat. Control*, vol. 43, no. 5, pp. 619–630, May 1998.

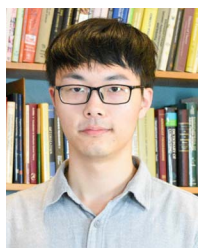

Feifan Chen (Student Member, IEEE) received the B.S. and M.S. degrees in electrical engineering from the Harbin Institute of Technology, Harbin, China, in 2019 and 2021, respectively. He is currently working toward the Ph.D. degree in electrical engineering with the School of Electrical Engineering and Computer Science, KTH Royal Institute of Technology, Stockholm, Sweden.

His research interests include modeling and control of grid-connected converters, stability assessment and dynamic analysis of power-electronic-dominated power systems.

Sei Zhen Khong (Senior Member, IEEE) received the Bachelor of Electrical Engi-neering degree (with first class honours) and the Ph.D. degree in electrical engineering from the University of Melbourne, Melbourne, Australia, in 2008 and 2012, respectively.

He held research positions with the Department of Electrical and Electronic Engineering, University of Melbourne, Australia, Department of Automatic Control, Lund University, Sweden, Institute for Mathematics and its Applications, University of Minnesota Twin Cities, USA, and Department of Electrical and Electronic Engineering, University of Hong Kong, China. He is currently with the Department of Electrical Engineering, National Sun Yat-sen University, Taiwan. His research interests include network control, systems theory, and optimization with applications to systems biology, power systems, and electromechanical systems.

Lennart Harnefors (Fellow, IEEE) received the M.Sc., Licentiate, and Ph.D. degrees in electrical engineering from the Royal Institute of Technology (KTH), Stockholm, Sweden, in 1993, 1995, 1997, respectively, and the Docent (D.Sc.) degree in industrial automation from Lund University, Lund, Sweden, in 2000.

From 1994 to 2005, he was with Mälardalen University, Västerås, Sweden, from 2001 as a Professor of electrical engineering. From 2001 to 2005, he was, in addition, a part-time Visiting Professor of electrical drives with Chalmers University of Technology, Gothenburg, Sweden. In 2005, he joined ABB, HVDC Product Group, Ludvika, Sweden, where, among other duties, he led the control development of the first generation of multilevel-converter HVDC Light. In 2012, he joined ABB, Corporate Research, Västerås, where he was appointed as a Senior Principal Scientist in 2013 and as a Corporate Research Fellow in 2021. He is, in addition, a part-time Visiting Professor with Aalto University, Espoo, Finland. His research interests include control and dynamic analysis of power electronic systems, particularly grid-connected converters and ac drives.

Dr. Harnefors is an Editor of IEEE JOURNAL OF EMERGING AND SELECTED TOPICS IN POWER ELECTRONICS. He was the recipient of the 2020 IEEE Modeling and Control Technical Achievement Award.

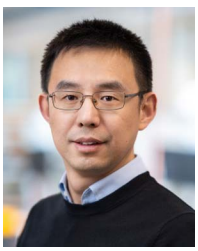

Xiongfei Wang (Fellow, IEEE) received the B.S. degree from Yanshan University, Qinhuangdao, China, in 2006, the M.S. degree from Harbin Institute of Technology, Harbin, China, in 2008, both in electrical engineering, and the Ph.D. degree in energy technology from Aalborg University, Aalborg, Denmark, in 2013.

From 2009 to 2022, he was with Aalborg University, where he became an Assistant Professor in 2014, an Associate Professor in 2016, a Professor and the founding Leader of Electronic Power Grid (eGRID) Research Group in 2018. From 2022, he has been a Professor with KTH Royal Institute of Technology, Stockholm, Sweden, and a Parttime Professor with Aalborg University. Form 2023, he has been a Visiting Professor with Hitachi Energy Research Center, Vasteras, Sweden. His research interests include modeling and control of power electronic converters, stability and power quality of power-electronic-dominated power systems, and high-power electronic systems.

Dr. Wang currently serves as Executive Editor for IEEE TRANSACTIONS ON POWER ELECTRONICS LETTERS and as Associate Editor for IEEE JOURNAL OF EMERGING AND SELECTED TOPICS IN POWER ELECTRONICS. From 2025, he will be the Editor-in-Chief for IEEE TRANSACTIONS ON POWER ELECTRONICS LETTERS. He was arecipient of 11 IEEE Prize Paper Awards, the 2016 AAU Talent for Future Research Leaders, the 2018 IEEE Richard M. Bass Outstanding Young Power Electronics Engineer Award, the 2019 IEEE PELS Sustainable Energy Systems Technical Achievement Award, and the 2022 Isao Takahashi Power Electronics Award.

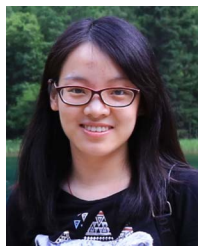

Dan Wang (Member, IEEE) received the B.S. degree in automation from Hangzhou Dianzi University, Hangzhou, China, in 2014, and the M.Phil. and Ph.D. degrees in electronic and computer engineering from the Hong Kong University of Science and Technology, Hong Kong, in 2016 and 2020, respectively.

She is currently a Postdoc with KTH Royal Institute of Technology. From January to July 2018, she was a Visiting Scholar with the Coordinated Science Laboratory, University of Illinois at Urbana Champaign, Urbana, IL, USA. Her research interests include systems and control theory, dynamical networks, network science, and control of epidemics.

Henrik Sandberg (Fellow, IEEE) received the M.Sc. degree in engineering physics and the Ph.D. degree in automatic control from Lund University, Lund, Sweden, in 1999 and 2004, respectively.

He is currently a Professor with the Division of Decision and Control Systems, KTH Royal Institute of Technology, Stockholm, Sweden. From 2005 to 2007, he was a Postdoctoral Scholar with the California Institute of Technology, Pasadena, USA. In 2013, he was a Visiting Scholar with the Laboratory for Information and Decision Systems (LIDS) at MIT, Cambridge, USA. He has also held visiting appointments at the Australian National University and the University of Melbourne, Australia. His current research interests include security of cyber-physical systems, power systems, model reduction, and fundamental limitations in control.

Dr. Sandberg was a recipient of the Best Student Paper Award from the IEEE Conference on Decision and Control in 2004, an Ingvar Carlsson Award from the Swedish Foundation for Strategic Research in 2007, and a Consolidator Grant from the Swedish Research Council in 2016. He has served on the editorial boards of IEEE TRANSACTIONS ON AUTOMATIC CONTROL and the *IFAC Journal Automatica*.

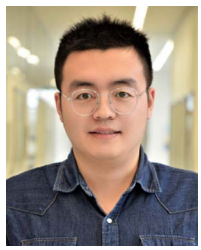

Liang Zhao (Member, IEEE) received the B.S. and M.S. degrees in electrical engineering from the Harbin Institute of Technology, Harbin, China, in 2018 and 2020, respectively, and the Ph.D. degree in power electronic systems from the Department of Energy, Aalborg University, Aalborg, Denmark, in 2024.

He is currently a Postdoctoral Researcher with the KTH Royal Institute of Technology, Stockholm, Sweden. His research interests include modeling and control of power electronic converters and systems.

Dr. Zhao was the recipient of the best paper award for 2023 Wind and Solar Integration Workshop.

Mikko Routimo (Member, IEEE) received the M.Sc. (El. Eng.), Lic.Tech., and D.Sc. (Tech.) degrees in electrical engineering from Tampere University of Technology, Tampere, Finland, in 2002, 2005, and 2009, respectively.

He joined ABB Oy Drives, Helsinki, Finland, in 2008, where he was appointed as a Senior Principal Engineer in 2022. From 2017 to 2022 he was, in addition, a part-time Professor of Practice with the School of Electrical Engineering, Aalto University, Espoo, Finland. His research interests include control of power electronic converters and systems.

Jarno Kukkola received the B.Sc. (Tech.), M.Sc. (Tech.), and D.Sc. (Tech.) degrees in electrical engineering from the Aalto University, Espoo, Finland, in 2010, 2012, and 2017, respectively.

He is currently an R&D Principal Engineer with ABB Oy Drives, Helsinki, Finland. His research interests include control systems and grid-connected converters.

Kin Cheong Sou (Member, IEEE) received the Ph.D. degree in electrical engineering and computer science at Massachusetts Institute of Technology, Cambridge, MA, USA, in 2008.

From 2008 to 2010, he was a Postdoctoral Researcher with Lund University, Lund, Sweden. From 2010 to 2012 he was a Postdoctoral Researcher with KTH Royal Institute of Technology, Stockholm, Sweden. Between 2013 and 2016, he was an Assistant Professor with the Department of Mathematical Sciences, Chalmers University of Technology and the University of Gothenburg, Sweden.

Dr. Sou is currently an Associate Professor with the Department of Electrical Engineering at the National Sun Yat-sen University, Taiwan. His research interests include decision-making and computation techniques for power systems applications.

Karl Henrik Johansson (Fellow, IEEE) received the M.Sc. degree in electrical engineering and the Ph.D. degree in automatic control from Lund University, Lund, Sweden.

He is Swedish Research Council Distinguished Professor in electrical engineering and computer science with KTH Royal Institute of Technology in Sweden and Founding Director of Digital Futures. He has held visiting positions at UC Berkeley, Caltech, NTU and other prestigious institutions. His research interests focus on networked control systems and cyber-physical systems with applications in transportation, energy, and automation networks.

Prof. Johansson was a recipient of numerous best paper awards and various distinctions from IEEE, IFAC, and other organizations, for his scientific contributions. He has been awarded Distinguished Professor by the Swedish Research Council, Wallenberg Scholar by the Knut and Alice Wallenberg Foundation, Future Research Leader by the Swedish Foundation for Strategic Research. He has also a recipient of the triennial IFAC Young Author Prize and IEEE CSS Distinguished Lecturer. He is the recipient of the 2024 IEEE CSS Hendrik W. Bode Lecture Prize. His extensive service to the academic community includes being President of the European Control Association, IEEE CSS Vice President Diversity, Outreach & Development, and Member of IEEE CSS Board of Governors and IFAC Council. He has served on the editorial boards of Automatica, IEEE TAC, IEEE TCNS and many other journals. He has also been a member of the Swedish Scientific Council for Natural Sciences and Engineering Sciences. He is Fellow of the Royal Swedish Academy of Engineering Sciences.